The significance of low carbon bio-alcohols and bio-ketones fuels for clean propulsion systems

Doustdar, Omid; Zeraati-Rezaei, Soheil; Herreros, Jose Martin ; Martos, Francisco Javier ; Tsolakis, Athanasios; Wyszynski, Miroslaw Lech

Link to publication on Research at Birmingham portal

Full Length Article

The significance of low carbon bio-alcohols and bio-ketones fuels for clean propulsion systems

Omid Doustdar [a], Soheil Zeraati-Rezaei [a], Jose Martin Herreros [a], Francisco Javier Martos [b], Athanasios Tsolakis [a,*], Miroslaw Lech Wyszynski [a]

[a] *Department of Mechanical Engineering, School of Engineering, University of Birmingham, Birmingham B15 2TT, UK*
[b] *Escuela de Ingenieras Industriales, University of Malaga, c/Doctor Ortiz Ramos, s/n, 29071 Malaga, Spain*

A B S T R A C T

This experimental work investigates oxygenated bio-fuel component blends of butanol, pentanol and cyclo-pentanone with diesel on the combustion characteristics, gaseous emissions and particulate matter (PM). Furthermore, PM characteristics, including size distributions, morphology and nanostructure are investigated.

The oxygen content on the sustainable fuel blend components (bio-alcohols and bio-ketone) and the lower cetane number leading to a longer ignition delay, larger premixed combustion phase and high mean peak combustion temperature reduced the total number of particle concentration by up to 91%. Characterisation of particles demonstrated morphological and nanostructural alterations, such as the reduction in primary particle size that would lead to greater particle oxidation reactivity. Furthermore, the combustion of oxygenated blends showed a reduction in the total hydrocarbon emissions and an increase in NO_2 concentration. This research provides new knowledge to understand the effects of fuel properties on gaseous and particle emissions formation and characteristics. Overall this work demonstrates bio-alcohols and bio-ketones as low carbon fuels in unveiling strategies for vehicular emissions abatement.

1. Introduction

The automotive industry is undergoing developments to achieve greenhouse gas emission reduction targets globally. Regardless of current electrification plans, around 90 % of new cars sold in 2022 utilise internal combustion engines globally [1,2]. Additionally, transportation (including hybrid electric vehicles) should still cover a significant portion of the total biofuel demand (i.e., using renewable energies for a minimum of 14 % in road and rail transport by 2030) [3,4]. Integration between advanced fuels (such as carbon neutral fuels), advanced combustion and aftertreatment systems in the various propulsion system, including electrified powertrains such as hybrid electric vehicles [5], results in significantly lower emissions. For example, gasoline compression ignition (GCI) engines and their hybridisation [6] demonstrate high efficiency, lower fuel consumption compared to gasoline in spark ignition (SI) engines and low NO_x and particle emissions compared to diesel fuel in CI engines [7].

The molecular structure of biomass-derived bio-alcohols and bio-ketones as fuel candidates for low-emission vehicles [8], influences fuel ignition characteristics (e.g. ignition delay), spray and atomisation quality [9], combustion process (e.g. fraction of premixed/diffusion combustion, flame temperature [10] and heat release rate [11]), gaseous and particle emissions concentrations and characteristics [12]. Longer chain alcohols (i.e., butanol and pentanol) are gaining more attention as alternatives to be blended with diesel. This is due to their better miscibility, solubility, higher viscosity, better lubricity, higher calorific value, lower heat of vaporisation and higher hygroscopicity compared with short-chain alcohols (i.e., ethanol and methanol) [12,13].

In addition to bio-alcohols (butanol and pentanol), cyclopentanone and cyclopentanol are environmentally friendly and have great economic potential for practical application as alternative fuel [8,14]. According to carbon tracing, in these oxygenated cyclic compounds, the conversion rate on PM of OH carbon in molecular structure occupied 11 % less than in the ethanol [15]. Also, the fuel reactivity of cyclopentanol at low temperatures is very low, and the self-ignition tendency of cyclopentanol is lower than pentanol [16]. Studies on an optical engine indicated that improved spray and atomisation quality of oxygenated cyclic compounds leads to complete combustion with significantly lower soot emissions than diesel, biodiesel and esters [9].

Nomenclature

AC	Alternating current
B	Butanol
B20	Butanol 20 %+Diesel 80 % (v/v)
C	Atomic carbon
CAD	Crank angle degree
CFPP	Cold filter plugging point
CH_2O	Formaldehyde
CH_3OH	Methanol
CH_3CHO	Acetaldehyde
CH_4	Methane
C_2H_2	Acetylene
C_2H_4	Ethylene
C_2H_5OH	Ethanol
C_2H_6	Ethane
C_3H_6	Propylene
C_4H_9OH	Butanol
$C_5H_{11}OH$	Pentanol
CI	Compression ignition
CO	Carbon monoxide
CO_2	Carbon dioxide
COV	Coefficient of variation
CP	Cyclopentanol
CP20	Cyclopentanol 20 %+Diesel 80 % (v/v)
CPK	Cyclopentanone
CPK20	Cyclopentanone 20 %+Diesel 80 % (v/v)
d_{002}	Fringe separation distance
D100	Diesel 100 %
D_f	Fractal dimension
d_{po}	Average diameter of primary particles
d_{SMPS}	median diameter of particles
DOC	Diesel oxidation catalyst
DPF	Diesel particulate filter
EDS	Energy dispersive spectrometer
EGR	Exhaust gas recirculation
EN	European Standards
EU	European Union
fps	Frame per second
FTIR	Fourier transform infrared
GCI	Gasoline compression ignition
H	Atomic hydrogen
H_2	Hydrogen
HC	Hydrocarbons
HCCI	Homogenous charge compression ignition
HEPA	High-efficiency particle arrestance
HR	high-resolution
HRR	Heat release rate
IC	Internal combustion
IMEP	Indicated mean effective pressure
ISFC	Indicated specific fuel consumption
ISO	International Standard Organization
ITE	Indicated thermal efficiency
L_c	Fringe length
LHV	Lower heating value
MNC	Maximum number concentration
MND	Median diameter
ms	mili second
N_2	Nitrogen
N_2O	Nitrous oxide
NEDC	New European driving cycle
nm	nanometer
NO	Nitric oxide
NO_2	Nitrogen dioxide
NO_x	Nitrogen oxides
O	Atomic oxygen
O_2	Oxygen
OH	Hydroxyl radicals
P	Pentanol
P20	Pentanol 20 %+Diesel 80 % (v/v)
PM	Particulate matter
PN	Particulate number
ppm	Parts per million
PSD	Particle size distribution
R_g	Radius of gyration
RPM	Revolutions per minute
SI	Spark ignition
SMPS	Scanning Mobility Particle Sizer
TDC	Top dead centre
TEM	Transition electron microscope
THC	Total hydrocarbons
T_f	Tortuosity
ULSD	Ultralow sulphur diesel
TNC	Total number concentration
θ	Crank angle (deg)
λ	Specific (relative) air–fuel ratio
°C	degree Celsius

The oxygen content in fuels with different molecular structures improves the soot oxidation reactivity [17], improving diesel particulate filter (DPF) function and durability by decreasing the regeneration temperature and lowering the intensity of soot burn-off cycles. In addition to particle concentration and size, high-resolution transition electron microscope (HR-TEM) techniques have been used to study particle morphology and nanostructure. Particle morphology can influence the filtration and regeneration processes of the DPF with an impact on the exhaust backpressure and engine fuel economy. Additionally, the porosity and permeability of PM are related to the primary particle diameter and the number of primary particles per agglomerate, which can influence the soot oxidation reactivity [18]. The soot oxidation rate depends on the aggregate surface area to volume ratio, which is inversely proportional to the primary particle diameter [19]. Soot nanostructure is related to particle formation in the combustion chamber and initial fuel properties [20].

Additionally, soot surface chemistry, strongly linked to soot's environmental and health impact, depends on its morphology and nanostructure [21]. Most of the literature presents the qualitative characterisation of PM emitted by diesel engines. Therefore, this work provides a new understanding of the influence of the molecular structure of bio-alcohols and bio-ketones (i.e., diesel blended with butanol, pentanol, cyclopentanol and cyclopentanone) on combustion, gaseous emissions, and particle emissions characteristics. These new findings enable to technically assess their potential in terms of engine performance and exhaust emissions (both regulated and non-regulated) of those bio-alcohols and bio-ketones as alternative and renewable fuel blending components for CI engines and assisting future powertrains to meet ever more stringent emission regulations. Lastly, this investigation enriches the research on the energy utilisation of biomass conversion and promotes alternative renewable fuels in current engines.

2. Methodology

The experimental work is carried out in a single-cylinder diesel engine running on neat diesel and four different fuels. In the present study,

based on a previously published work on fuel properties [8], B20, P20, CP20, and CPK20 were prepared by blending diesel with 20 % v/v of each fuel candidate (butanol, pentanol, cylopentanol and cyclo-pentanone, respectively).

2.1. Engine test and combustion analysis

The engine used in this study is a modern four-stroke single-cylinder research diesel engine. The engine technical data and specifications are summarised in Table 1. This engine is water-cooled, EGR equipped and utilised a common rail direct fuel injection. An alternating current (AC) electric dynamometer was used to motor and load the engine. Fig. 1 shows a schematic diagram of the experimental setup.

An AVL GH13P pressure transducer mounted in the cylinder head was used to record in-cylinder pressure and an AVL FlexiFEM 2P2 to amplify its signal. Also, a digital shaft encoder producing 360 pulses per revolution measured the crankshaft position. The pressure and crank-shaft position data were combined to create an in-cylinder pressure trace. The temperatures at different points on the exhaust manifold were recorded using k-type thermocouples and a Pico Technology TC-08 thermocouple data logger. An airflow meter was used to measure the engine intake airflow and monitor the air/fuel ratio in all tested con-ditions. Then λ as a ratio of actual air/fuel to stoichiometric air/fuel ratio was calculated.

An in-house developed LabVIEW programme connected to a Na-tional Instruments PCI-6023E data acquisition device was used to monitor and control the engine operating conditions, such as injection pressure, timing and duration. The coefficient of variation (COV) of the IMEP for 200 cycles was monitored and kept below 4 % during the testing procedure to confirm combustion stability and minimise cyclic variability. The LabVIEW programme analyses the engine indicated mean effective pressure (IMEP) for each cycle. In-cylinder pressure data was pegged to have the same in-cylinder pressure at the bottom dead centre of the intake stroke and intake manifold. The net heat release rate was obtained with logged average in-cylinder pressure data in 200 engine-operating cycles. In addition to these, under the steady-state condition, combustion phasing (AHR-50), combustion duration and ignition delay, the engine's fuel consumption and its corresponding indicated specific fuel consumption (ISFC) and the indicated thermal efficiency (ITE) of the tested conditions was calculated.

The engine operating conditions are summarised in Table 2; 1500 rpm with 2 bar and 4 bar IMEP was selected as the engine rotational speed and load. These steady-state engine-operating conditions were set to assess engine performance and emissions in a target new European driving cycle test [22]. Engine loads (defined as indicated mean effective pressure (IMEP)) were chosen to reproduce low to medium loads. The common rail fuel injection pressure was set at 550 and 650 bar based on operating conditions. The pilot fuel injection was set to start at 15 °bTDC with an injection duration of 0.150 ms, whereas the main injection started at 3 °bTDC with injection durations of around 0.443 ms (it is variable based on the fuel properties, i.e., higher values for oxygenated components) to maintain constant IMEP. In the studied cases, there is not any post fuel injection.

2.2. Gaseous emissions analysis and particle number concentration

An MKS MultiGas 2030 Fourier Transform Infrared (FTIR) spec-troscopy analyser was used to analyse the engine's exhaust gaseous emissions. Legislated emissions, including total unburnt hydrocarbons (THC), carbon oxides (CO and CO_2) and nitrogen oxides (NO_x: NO and NO_2), are analysed. Also, unregulated HC species such as methane (CH_4), ethane (C_2H_6), ethylene (C_2H_4), propylene (C_3H_6), and acetylene (C_2H_2) and formaldehyde (CH_2O) are measured. In the gaseous emis-sions analysis, FTIR measures the gaseous species in ppm (v/v) format, then converted into the brake-specific format (g/kWh).

A TSI Scanning Mobility Particle Sizer (SMPS) was employed to measure the particle emissions' mobility size and number distribution. The SMPS has a 3080 electrostatic classifier, a 3081 differential mobility analyser and a 3775-condensation particle counter. To dilute the sample and avoid nucleation and condensation of moisture or hydrocarbon, the dilution ratio (1:25) was controlled to have the same condition for the entire testing matrix. The measurements were carried out using a heated sampling line with a temperature of 191 °C to avoid hydrocarbon condensation and nucleation.

2.3. Morphological analysis of particle emissions

For particle morphology and nanostructure, samples were collected from the exhaust gas stream onto a Formvar/Carbon film supported on a 3 mm diameter copper grid, supplied by TAAB Laboratories Ltd. These particulates were analysed using high-resolution transmission electron microscopy (HR-TEM) with a FEI Talos^{TM} F200X S/TEM coupled to a FEI Ceta 16M^{TM} camera to obtain the micrographs of particle agglomerates with a high resolution up to 0.12 nm at a fast rate of 25 fps. Exhaust particle and gas concentrations were measured at the same sampling points for consistency. Two grids were obtained experimentally from each test condition to minimise errors and uncertainty in sampling.

The morphological and nanostructural parameters, such as radius of gyration (R_g), the diameter of primary particles (d_{po}), fractal dimension (D_f), fringe length (L_c), fringe separation distance (d_{002}) were analysed from the HR-TEM micrographs using a bespoke digital analysis software in Matlab®. The conversion from pixels to nanometres was calibrated by comparison with standard latex spheres shadowed with gold.

For the morphology parameters (R_g, d_{po} and D_f), at least 30 ag-glomerates were photographed and analysed with the method proposed by Lapuerta et al. and Martos et al. [23–25]. Also, with high-resolution images of agglomerate obtained from each grid, the nanostructural pa-rameters (d_{002} and L_c) were analysed with the method proposed by Yehliu et al. [26]. These developed methods have already proven effective and reliable techniques for morphology and nanostructure characterisation of particulate matter.

3. Results and discussion

3.1. Combustion analysis

All fuel blends have been tested at the same operating conditions defined by engine speed and IMEP. The calculated λ values were approximately constant for all the tested fuel blends (Table 3). This enables majorly attributing the fuel effects on combustion, gaseous and particulate matter emissions to fuel itself (properties) rather than being compared at different operation conditions.

The use of oxygenated fuel blends increases ISFC compared to the baseline diesel fuel combustion. Accordingly, longer fuel-injection du-rations were recorded (section 2.1) for oxygenated fuel blends compared to diesel to maintain the same engine IMEP condition. ITE is calculated to take into account the heating value of the fuels. There are no signif-icant differences between all the fuels in ITE at medium load (4 bar IMEP), which indicates that the increases in ISFC with the use of oxygenated fuel blends are due to their smaller heating value. However,

Table 1
Test engine specifications.

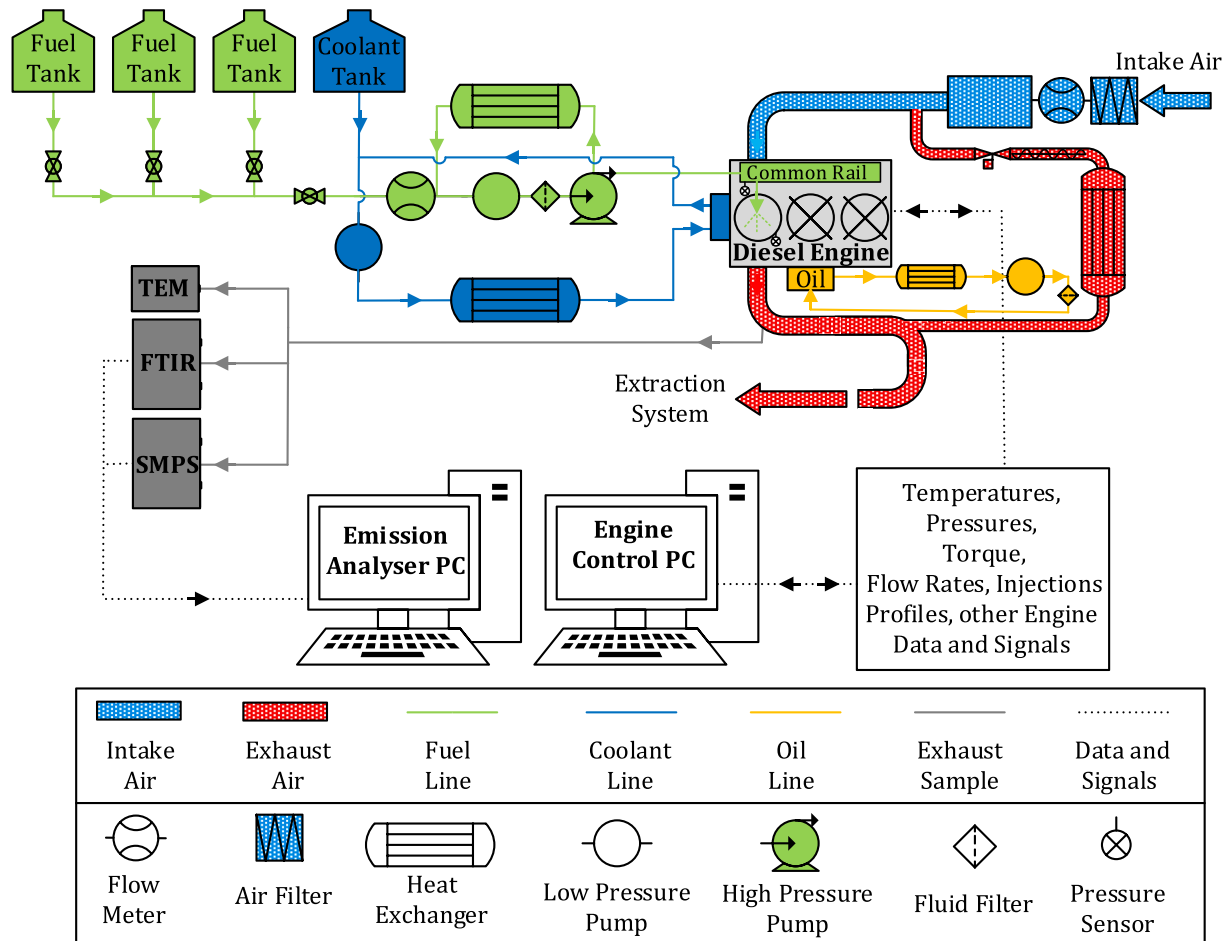| Engine specification	Data
Number of Cylinders	1
Bore	84 mm
Stroke	90 mm
Connecting Rod Length	160 mm
Displacement Volume	499 cm^3
Compression Ratio	16.1:1
Maximum Injection Pressure	1500 bar

Fig. 1. Experimental set-up diagram.

Table 2
Engine test conditions abbreviations.

Test abbreviation	Fuel blends with diesel (%v/v)	Engine speed (rpm)	Fuel injection pressure (bar)	IMEP (bar)	Injection timing bTDC-(CAD)	
					Pre	Main
D100L	Diesel 100%	1500	550	2	15	3
B20L	Butanol 20%	1500	550	2	15	3
P20L	Pentanol 20%	1500	550	2	15	3
CP20L	Cyclopentanol 20%	1500	550	2	15	3
CPK20L	Cyclopentanone 20%	1500	550	2	15	3
D100M	Diesel 100%	1500	650	4	15	3
B20M	Butanol 20%	1500	650	4	15	3
P20M	Pentanol 20%	1500	650	4	15	3
CP20M	Cyclopentanol 20%	1500	650	4	15	3
CPK20M	Cyclopentanone 20%	1500	650	4	15	3

at low load (2 bar IMEP), oxygenated components result in a lower ITE (reduction of 5 % and 11.7 % for B20 and CP20, respectively) compared to diesel, which is due to other fuel properties such as latent heat of evaporation, cetane number, viscosity, density and oxygen content [27,28].

Comparing fuel components, the high oxygen content, low viscosity, and low surface tension of butanol/diesel (B20) leads to the highest ITE of the engine. Also, the lower boiling point of butanol compared to other oxygenated fuels [8], implies better spray characteristics and fuel atomisation, enhancing the combustion process. Moreover, among tested oxygenated components, ITE is generally lower for cyclopentanol/diesel (CP20) and pentanol/diesel (P20) blends as a result of

their higher viscosity and density potentially worsening fuel vaporisation, atomisation and mixing with air and their lower oxygen content compared to other fuel blends [27].

The trends in the exhaust temperature can be related to combustion duration (duration between AHR-10 to AHR-90, Fig. 2). Based on net cumulative heat release analysis, CP20 has the longest combustion duration leading to the highest exhaust temperature, while CPK20 has the shortest combustion duration leading to the lowest exhaust temperature. It can be concluded that the exhaust gas temperature variation is more related to the heating value of the fuels at low load. However, at a medium load, the temperature is related to the cetane number and latent heat of evaporation, leading to changes in ignition delay [29].

Table 3
Summarised combustion analysis for test conditions.

Test abbreviation	λ	ISFC (kg.kwh^{-1})	ITE (%)	Exhaust temperature (°C)
D100L	3.25 ± 0.10	0.294 ± 0.01	26.67 ± 0.5	226 ± 3
B20L	3.10 ± 0.10	0.326 ± 0.01	25.35 ± 0.5	231 ± 3
P20L	3.10 ± 0.10	0.332 ± 0.01	24.64 ± 0.5	227 ± 3
CP20L	3.00 ± 0.10	0.348 ± 0.01	23.55 ± 0.5	237 ± 3
CPK20L	3.05 ± 0.10	0.332 ± 0.01	24.75 ± 0.5	225 ± 3
D100M	1.85 ± 0.10	0.260 ± 0.01	30.08 ± 0.5	342 ± 3
B20M	1.90 ± 0.10	0.264 ± 0.01	31.28 ± 0.5	331 ± 3
P20M	1.85 ± 0.10	0.272 ± 0.01	30.11 ± 0.5	338 ± 3
CP20M	1.85 ± 0.10	0.268 ± 0.01	30.58 ± 0.5	337 ± 3
CPK20M	1.85 ± 0.10	0.270 ± 0.01	30.28 ± 0.5	336 ± 3

High oxygen content in the fuel, which increases oxygen-rich regions in the combustion chamber, can lead to higher peak in-cylinder temperatures and exhaust gas temperature, as it is observed at low load conditions. The same results were reported by Atmanli [13]. However, a dissimilar finding reported by Cheung et al. [30]. They claimed that a decrease in exhaust gas temperature for alcohols blends was due to lower calorific value and higher latent heat of evaporation. Thus, the molecular structure of fuels has a dominant influence over fuel properties itself.

The in-cylinder pressure and net heat release rate versus crank angle degree for the five different tested fuels at constant injection timing and two engine loads of 2 bar and 4 bar IMEP are shown in Fig. 2 (a) and (b), respectively. The oxygenated fuel blends have a longer ignition delay, which shifted the peak heat release rate compared to diesel fuel combustion (Fig. 2, first combustion event). It can be seen that the order of duration in ignition delay for pre-injection are CPK20 > B20 > P20 > CP20 > D100.

Comparing straight-chain alcohols, the lower cetane number of butanol compared to pentanol leads to longer ignition delay, higher

rates of premixed combustion and high peak in-cylinder pressure [28]. The lower ignition delay with increasing carbon chain length (butanol-C_4 to pentanol-C_5) agrees with E. Koivisto et al. [31]. It is suggested that this decrease in ignition delay with increasing carbon chain length is partly due to the increase in the number of secondary C–H bond and the more exceptional ability of the fuel peroxy radicals to isomerise. The higher number of easily abstracted secondary H atoms results in faster overall H-abstraction and faster radical pool formation, reducing the ignition delay. This is also in agreement with Schonborn et al. [32], reports that an increase of the carbon chain length attached to the OH in the alcohols decreases the ignition delay.

The cyclopentanol/diesel fuel blend (CP20) has the shortest ignition delay between the tested blends. Our findings show that the cyclic structure provides an exceptional ability to fuel peroxy radicals to isomerise. Except for cetane number, most of the cyclopentanol properties are almost similar to diesel [8]. These properties make CP20 combustion behaviour almost similar to diesel (Fig. 2). Cyclopentanone resulted in the largest increase in the ignition delay being in accordance to (i) its low cetane number [8], (ii) higher polarity leading to lower volatility [31] and (iii) high heat of evaporation (cooling effect) [12]. The oxygen in the carbonyl group of cyclopentanone on H-abstraction led to the longest ignition delay among tested fuels. Also, the higher electronegativity of the oxygen atom compared to that of a hydrogen atom affects the strengths of the nearby C–H bonds in the fuel molecules [31]. So, H-abstraction from the neighbouring secondary carbon atom in cyclopentanone becomes more accessible than the abstraction of the corresponding secondary hydrogen atom of pentanol and cyclopentanol. So, these changes in difficulty of the overall H-abstraction from ketone compared to alcohol increase ignition delay duration. Besides H-abstraction, the ignition delay of cyclopentanone is also likely to be affected by the further reactions of fuel radicals. These radicals react with oxygen into ketonyl peroxy radicals [31]. Thus isomerisation of ketonyl peroxy radicals become more challenging than that of alkyl peroxy radicals in alkane combustion. The isomerisation of the fuel peroxy radicals initiates the low-temperature branching reactions [31]. Therefore the lower ability of ketone (CPK20) to undergo this reaction is expected to contribute to its higher ignition delays compared to other tested fuels (Fig. 2).

3.2. Gaseous emissions analysis

3.2.1. Unburnt hydrocarbon emissions

As the engine load increases, the rise of in-cylinder temperature leads
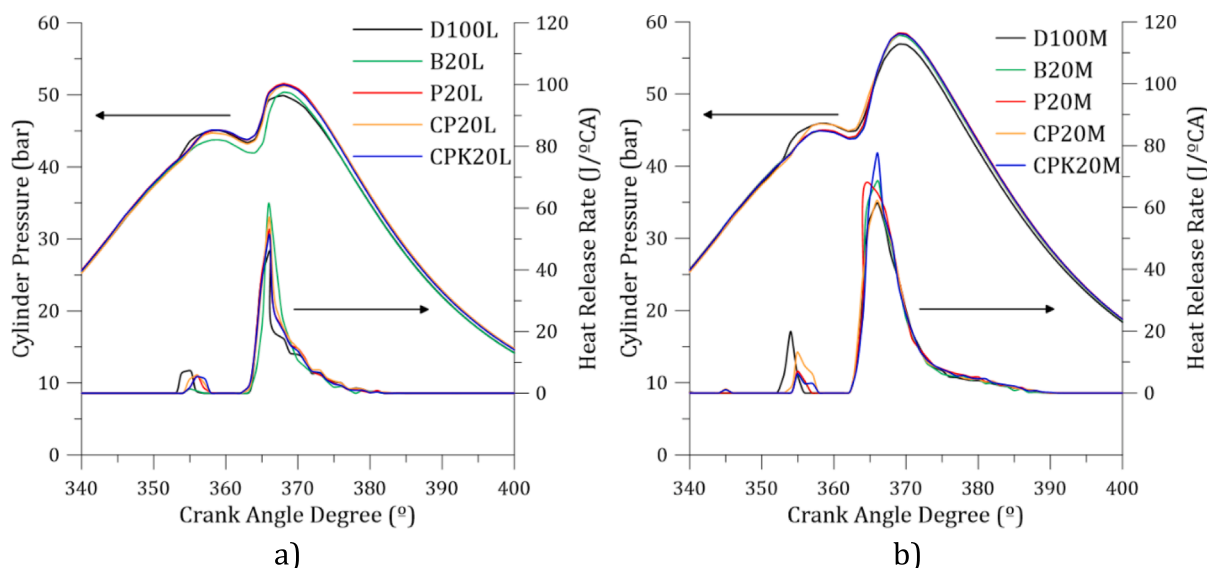
a)

b)

Fig. 2. In-cylinder pressure and heat release rate at a) 2 bar IMEP and b) 4 bar IMEP.

to complete combustion, which is beneficial in total hydrocarbon (THC) reduction [29] (Fig. 3). Lower THC emissions were obtained for the oxygenated fuel blends compared to those emitted by the diesel fuel combustion at both engine-operating loads (Fig. 3). The reductions in HC emissions can be explained due to (i) oxygen presence in alternative fuel components [12,17], (ii) shorter carbon chain length compared to diesel fuel molecule, (iii) increase of ignition delay time leading to a higher proportion of premixed combustion enhancing fuel–air mixing and increasing in-cylinder pressure (Fig. 2) and temperature [33].

Comparing straight-chain alcohols, the lower oxygen mass fraction and higher viscosity of pentanol with longer carbon chain length than butanol result in higher THC emissions [13]. The higher viscosity of pentanol worsens atomisation and spray characteristics compared to butanol, particularly at low load which fuel is injected with lower pressure.

Cyclopentanol with the highest viscosity among these oxygenated fuel blends leading to the highest THC emissions (and highest medium-heavy HCs) at low load engine operation due to the low in-cylinder temperature and pressure. In contracts, cyclopentanol has the lowest THC emissions at a higher load because fuel injected with high pressure and in-cylinder temperature and pressure are high. Also, the lowest viscosity of cyclopentanone among tested fuels and high oxygen content leads to the lowest total hydrocarbons emissions, probably due to the efficient breakdown and partial oxidation of the fuel.

From Fig. 4, it can be seen that the distribution of unburnt hydrocarbon species mainly composed of medium-heavy hydrocarbons (such as alkanes, alkenes and aromatics). These hydrocarbon emissions could mostly come from unburnt diesel fuel itself, including 1,3 butadiene, benzene, toluene and xylene emissions as most reported hydrocarbons from diesel engine exhaust [30]. It is evident that the amount of oxygen
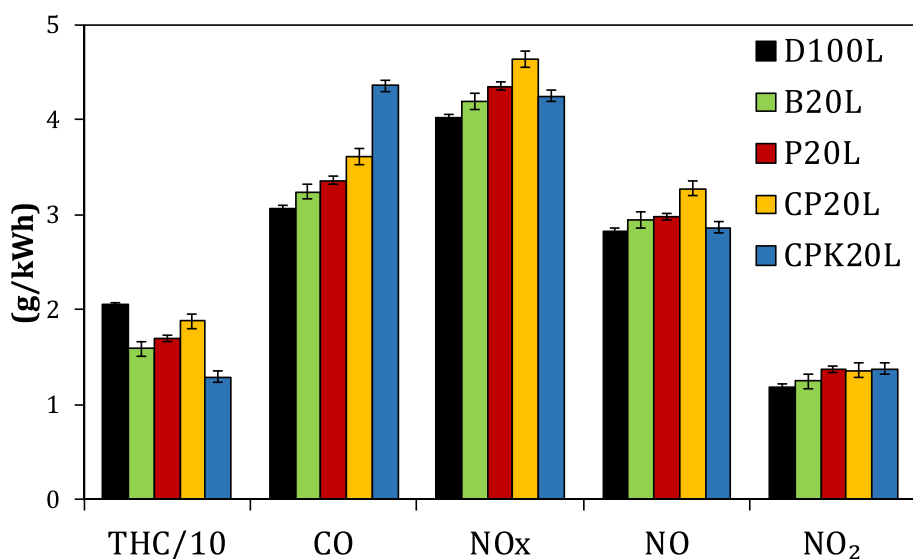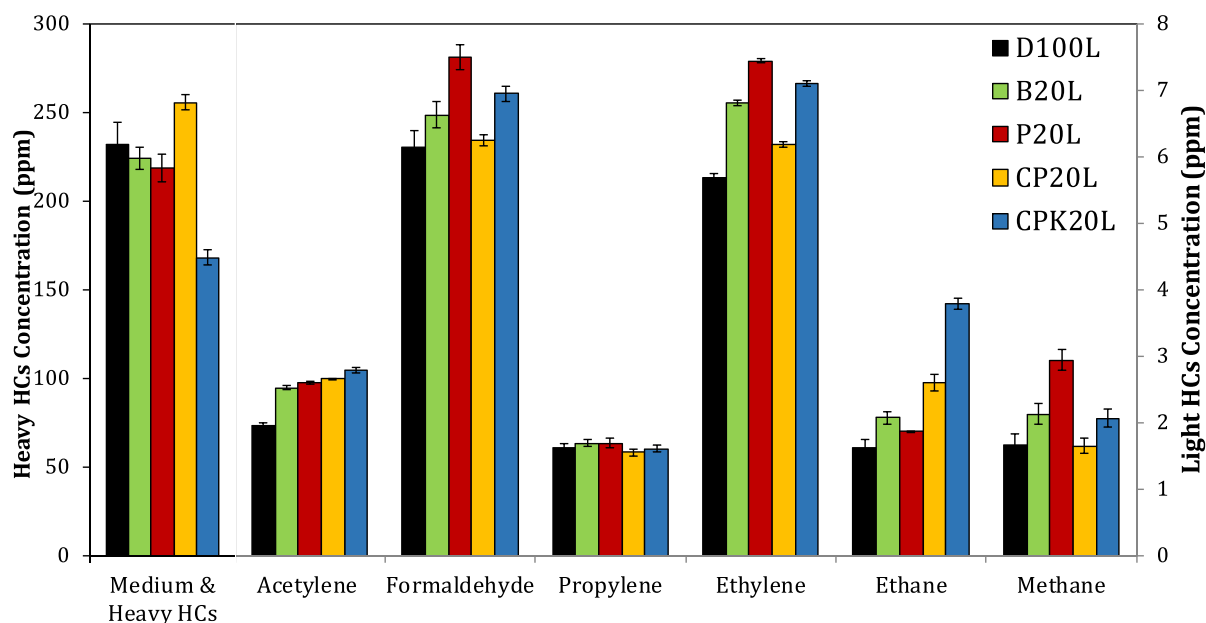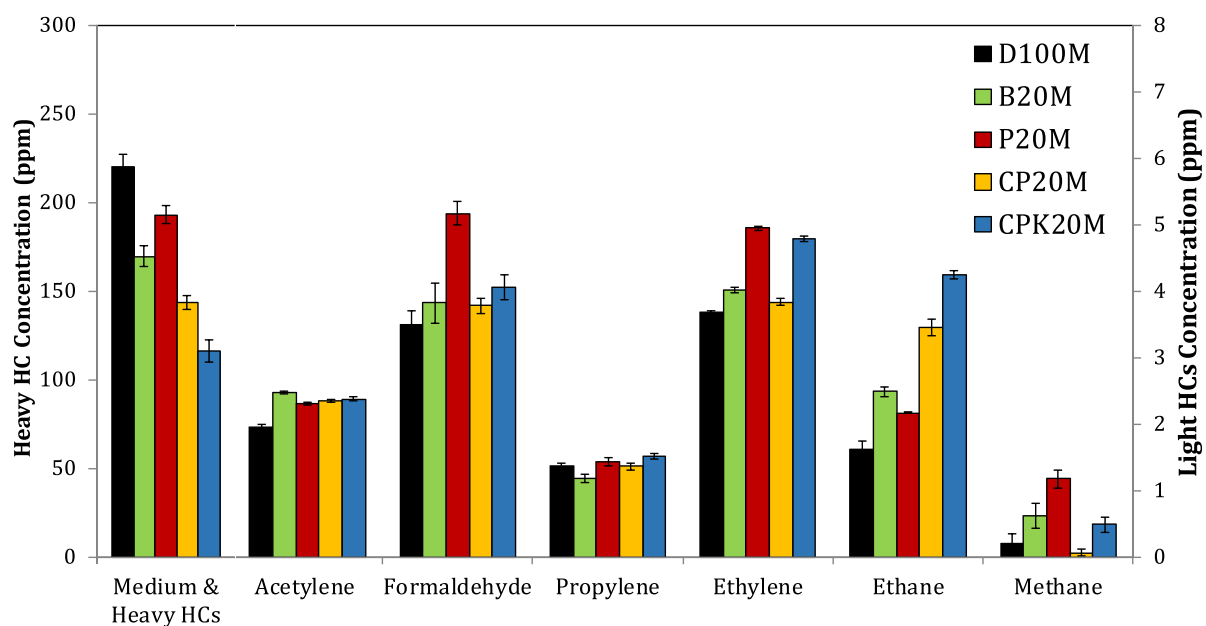

a)
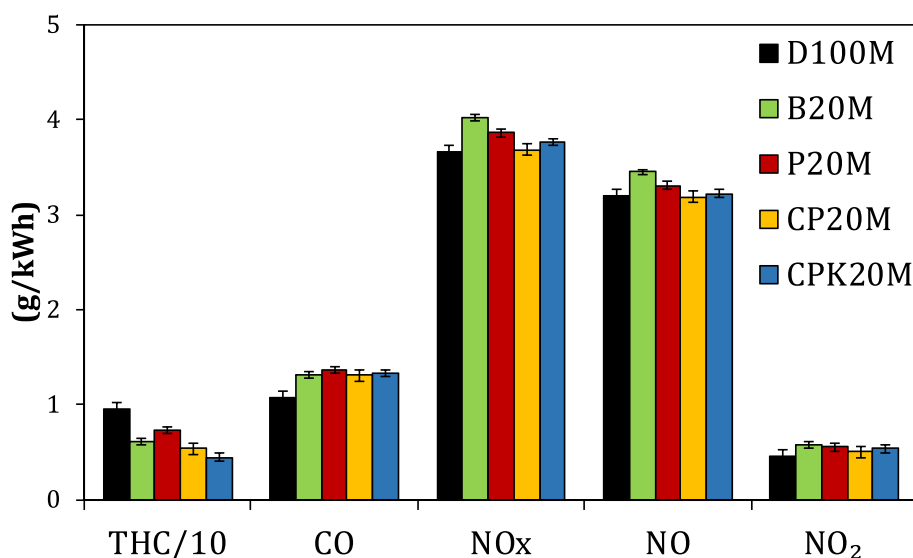
b)

Fig. 3. Total gaseous emissions at a) 2 bar IMEP and b) 4 bar IMEP.

a)

b)

Fig. 4. Hydrocarbon emissions speciation at a) 2 bar IMEP and b) 4 bar IMEP.

content, the chemical property of fuel, and viscosity directly affect medium-heavy hydrocarbon concentration [34]. Variation in medium-heavy hydrocarbons can be due to (i) presence of oxygen to improve combustion and promote the degradation of HCs, and (ii) presence of unsaturated HCs lead to the formation of aromatics and polycyclic aromatic hydrocarbons (PAHs). Also, oxygenated fuels have a dilution effect on the aromatics precursors leading to a reduction of aromatics among medium-heavy HCs emissions [30].

Light hydrocarbons, both saturated (such as methane and ethane) and unsaturated species (such as ethylene, propylene, acetylene and formaldehyde) being the small proportion. In general, there is only a slight decrease in the contribution of light HCs for all tested fuels with

increasing the engine load. Compared to diesel fuel, the short-chain structure of alternative fuels leads to a high percentage of light HCs emissions. Acetylene (C_2H_2), ethylene (C_2H_4) and propylene (C_3H_6) are the products of thermal cracking of fuel [35]. In general, olefin (C_nH2_n) has a higher tendency to further cleavages than paraffin (C_nH2_{n+2}), which justified the high content of ethylene and propylene in the exhaust gas in portion to methane and ethane [36]. There is no clear correlation between oxygen content in the fuel and light HCs because olefin and paraffin are the most unspecific products of fuel thermal cracking that are always found with similar quantities from exhaust [36]. Formaldehyde (CH_2O) is the simplest form of aldehyde group from internal combustion engines exhaust, which is the main intermediate

products of hydrocarbons or oxygenated compounds in the fuel [35,37]. At low load, because of the lean region in the engine amount of formaldehyde is a bit higher [37]. The distribution of formaldehyde in oxygenated fuel blend exhausts increase compared with the baseline diesel (Fig. 4) due to the oxygen content and higher H/C ratio in fuel molecular structure. The high availability of H in the exhaust will promote reaction with CO to form formaldehyde [35,37]. Also, alcohols are more reactive to form formaldehyde because of the high chance of oxygen [37]. As shown in Fig. 4, formaldehyde emissions are less than 8 ppm for all the fuels.

Hydrocarbon emissions are very dependent on engine operating conditions, engine performance, and aftertreatment systems; thus, it is a reasonably clear demonstration of the need for emission reduction technologies such as diesel oxidation catalysts (DOC). Thus, the combined use of alternative fuels and DOC can improve both regulated and unregulated emissions.

3.2.2. CO emissions

Carbon monoxide is produced by incomplete combustion of fuels containing carbon in fuel–air under-mixed and over-mixed regions within the combustion chamber. Fig. 3 shows, CO emissions at the medium IMEP (4 bar) are lower compared to low IMEP (2 bar) due to the higher in-cylinder pressure and temperature [29]. The combustion of the oxygenated fuel blends led to a slight increase in CO emissions at both loads compared with the baseline diesel [28,34]. The results show that with increasing engine load, the influence of the blended fuels in increasing CO emissions is reduced due to the higher combustion temperature; thus, the cooling effect of the oxygenated components is partially offset [38]. The higher concentration of CO emissions in the exhaust of the blended fuels can be due to two main factors: (i) the higher heat of evaporation of these fuels and (ii) their lower cetane number and viscosity. These factors can result in retarding a combustion phasing and a higher number of low temperature locally lean fuel–air mixture packets, enhancing CO formation rate and inhibiting its oxidation to CO_2 [12,13,29,33,38].

For straight-chain alcohols such as butanol and pentanol, an increase in the carbon chain length leads to a very slight increase in CO emissions due to a decrease in oxygen content [31]. The higher density and viscosity of cyclopentanol make larger fuel droplets that cause slower evaporation and higher CO emissions. Moreover, the lower H/C ratio of cyclopentanol and cyclopentanone [8] compared to straight-chain alcohols minimises OH radicals' development during oxidation. The hydroxyl component (OH radial) plays a significant role in converting CO to CO_2 [37]. This leads to higher CO emissions of CP20 and CPK20 compared with B20 and P20. As mentioned in section 3.2.1, efficient breakdown and partial oxidation of the fuel also led to relatively higher CO emissions. Moreover, the high heat of evaporation of cyclopentanone decreases the in-cylinder temperature and causes a cooling effect that promotes the formation of CO.

3.2.3. Nox emissions

NO_x formation in compression ignition engines depends on the in-cylinder temperature, flame temperature, available oxygen concentration and residence time in the reaction areas [31,38]. These parameters are functions of λ, fuel density, cetane number and fuel composition [39]. These positive and negative effects compete with each other and could lead to a variation of NO_x emissions in each tested condition. Fig. 3 presents, NO_x emissions at the medium IMEP (4 bar) are lower compared to low IMEP (2 bar) due to lower oxygen and nitrogen contents in the intake manifold (lower λ, Table 3) [39]. Engine-out NO_x emissions are generally slightly higher for oxygenated fuel blends than for diesel fuel combustion (Fig. 3). This is mainly due to the longer ignition delay of the oxygenated fuel blends than diesel, leading to a higher peak mean combustion temperature [11]. Also, the higher availability of oxygen may result in a higher flame temperature of the oxygenated fuel components than diesel. This result agreed with the review of several

previous studies, which have observed that oxygenated fuels tend to increase NO_x emissions [12,31,33].

NO_x emission at low load for butanol is lower than pentanol due to the low calorific value and high heat of evaporation [8] which reduces in-cylinder temperatures. At 4 bar IMEP, it can be seen that NO_x emission for P20 is less than B20, which is due to the result of the dominant influence of the oxygen content and lower cetane number of butanol over the cooling effect caused by the higher latent heat of evaporation of butanol. This was discussed earlier concerning longer ignition delay, too.

Shortest ignition delay of cyclopentanol at 2 bar IMEP combined with high flame temperature lead to high NO_x emission formation among tested fuels. However, at 4 bar IMEP positive effect of lower oxygen availability outweigh the negative impact of lower cetane number in terms of NO_x emissions. Cyclopentanone exhibits the lowest NO_x emissions among all the fuel blends (particularly at 2 bar IMEP). However, its premixed phase is larger due to longer ignition delay [33]. This could be due to a high enthalpy of evaporation, causing temperatures to decrease during combustion. The same observation can be seen at 4 bar IMEP for B20.

As presented in Fig. 3, the tested oxygenated fuel blends have higher NO_2 due to the oxygen content of the fuels. The cooling effect of oxygenated compounds may lead to lower gas temperature, and hence more NO is converted into NO_2 [40]. This high level of NO_2 could be beneficial due to its ability to oxidise soot at lower temperatures compared to oxygen (useful in regeneration of diesel particulate filters).

3.3. Particulate matter characteristics

3.3.1. Particle size distribution

The net formation of particles is mainly influenced by fuel structure, oxygen availability and in-cylinder temperature during the formation and oxidation process [41]. Fig. 5 shows the particle size distributions (PSD) of particulate matter (PM) from the combustion of the studied fuels. There is a lower particle concentration for most particle sizes from the combustion of oxygenated fuel blends compared to diesel fuel. The main reasons are the oxygen content in the fuel and the reduction in the diffusion combustion/premixed combustion rate [42]. The oxygen in oxygenated fuel components inhibits soot precursors and soot formation as well as enhances the oxidation of any newly particles formed during combustion and reduces its size. These results are in agreement with several other investigations stating that increasing the oxygen content in fuel leads to the reduction of particle emissions [12,27,31]. The higher volatility and lower cetane number of oxygenated compounds increases the proportion of premixed combustion with respect to diesel fuel, leading to lower particle formation [38]. This means that with a higher premixed phase, fuel-rich regions are reduced, leading to a reduction in the formation and growth of particulates [31,42].

There is reduction in the average particle size emitted from oxygenated fuels compare to diesel fuel combustion (Table 4). This could be seen as a disadvantage for oxygenated fuels because smaller size particles are more challenging to trap, they can transpire the respiratory and even circulatory system, they remain airborne in the atmosphere for much longer than larger particles, and they are more reactive due to their higher surface to volume ratio [33,43]. However, the main reason for the change in the median diameter is not a significant increase in the number of small size particles but a large reduction in the number of larger particle concentration (Fig. 5) [43]. This is also a result of the lower particle formation and a corresponding lower particle collision and the formation of larger particulate matter agglomerates [33,42].

The reduction of total particle number concentration for B20L, P20L, CP20L and CPK20L compared with D100L is 52 %, 36 %, 85 % and 91 %, respectively. The reduction of the number of particles for butanol than diesel is in good agreement with previous studies [12,17]. This is also attributed to the presence of oxygen in the hydroxyl group of the butanol
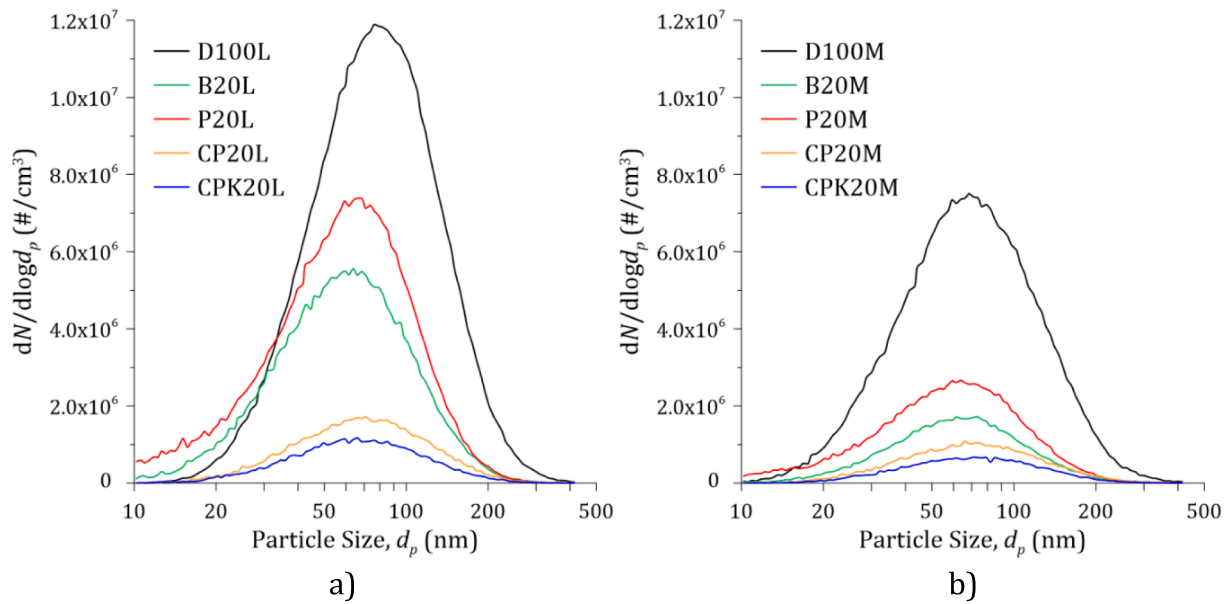
Fig. 5. Particle size distribution at a) 2 bar IMEP and b) 4 bar IMEP.

Table 4
Particle size distribution for tested fuels.

Test abbreviation	Total number concentration (#/cm³)	Maximum number concentration (#/cm³)	Median diameter (nm)
D100L	6.98×10^6	1.19×10^7	76.88
B20L	3.37×10^6	0.56×10^7	58.76
P20L	4.47×10^6	0.74×10^7	59.32
CP20L	1.03×10^6	0.14×10^7	68.25
CPK20L	0.65×10^6	0.12×10^7	65.67
D100M	4.76×10^6	7.51×10^6	67.78
B20M	1.01×10^6	1.72×10^6	63.01
P20M	1.67×10^6	2.67×10^6	58.56
CP20M	0.64×10^6	1.08×10^6	69.25
CPK20M	0.41×10^6	0.67×10^6	69.39

fuel blend affecting the reduction of soot formation and the improved rate of soot oxidation [17]. Also, it can be observed that soot particles follow the order of oxygen content in the blends and length of the carbon chain [27,38]. For straight chain alcohols, as the number of carbon atoms in the alcohols increases (i.e. its oxygen content decreases), higher levels of particle emissions are produced (P20 and B20 in Fig. 5) [27]. The lower soot reduction capability of pentanol compared to the other alternative fuel components could also be due to its high boiling temperature, which is difficult for fuel vaporisation and mixed with air, leading to local rich in fuel regions combustion chamber. This also plays a significant role in forming small particles (nucleation mode) [32]. Also, lower hydrogen to carbon ratio of pentanol than butanol could lead to a high tendency to soot formation [34,38].

Comparing CP20 (i.e. cyclopentanol as cyclic alcohol) and CPK20 (i. e. cyclopentanone as a ketone with carbonyl group), the higher produced particle emissions from CP20 could be due to the higher molecular weight and boiling point [32]. It is hypothesised that its lowest level of particle emissions in CPK20 is also due to its lowest cetane number, lowest viscosity, long ignition delay and thereby premixed phase, and high in-cylinder peak mean combustion temperature [31].

3.3.2. Particle morphology

Fig. 6 summarises particle morphology and nanostructure characteristics for all the studied fuels at both engine loads. The average radius of gyration and the average diameter of the primary particles (d_{po}) which compose the agglomerates increase with the engine load due to the increased fuel-rich regions enhancing particle formation and growth [44,45]. The radius of gyration of the particles emitted with the oxygenated fuels is smaller compared to those of the particles emitted with diesel fuel. This is a consistent trend with the lower average mobility diameter (d_{SMPS}) obtained for the oxygenated fuels. The oxygen content and the lower cetane rating of the oxygenated fuel components leading to a higher premixed combustion proportion inhibit particle formation and growth and enhances oxidation leading to a reduction in the concentration of large size agglomerates.

The primary particle diameter (d_{po}) (Fig. 6) of the particles emitted from the oxygenated compounds combustion (Fig. 5) is smaller than in the case of those emitted from diesel combustion at both engine loads. The reason of the smaller primary particle size is due to the lower number of particles and particle precursors slowing down particle surface growth as well as to the presence of chemically bound oxygen content in the hydroxyl and carbonyl group (alcohol and ketone), which decreases the dehydrogenation of the fuel at fuel-rich regions and enhances the oxidation of those particles. Similar results with oxygenated fuels have been reported elsewhere [12,45].

The mean fractal dimension (D_f), which is a parameter used to quantify the morphology of soot aggregates [17], for of all the studied conditions (load and fuel blends) are in the typical range of diesel particulates (1.5—1.8) which is characteristic of diffusion-limited aggregation mechanism growth. D_f has remained constant for particles emitted for B20 and P20 in both engine loads in comparison to those emitted by diesel fuel. However the fractal dimension for the particles emitted by from CP20 and CPK20 combustion has significantly increased with respect to diesel fuel particles. It is thought that the low level of particles emitted by CP20 and CPK20 has resulted in lower number of collisions between the particles leading to more compact agglomerates (Fig. 6). Furthermore, the enhancement of particle oxidation with oxygenated fuel blends could also lead to more compact agglomerates evidenced by the reduction of D_f [12].

3.3.3. Particle nanostructure

Particle nanostructure is quantified by average interlayer spacing (d_{002}) and graphene layer thickness (L_c). The lower the interlayer spacing (separation of the fringes), the greater the density of the soot. Fig. 6 shows that d_{002} generally decreases with increasing engine load
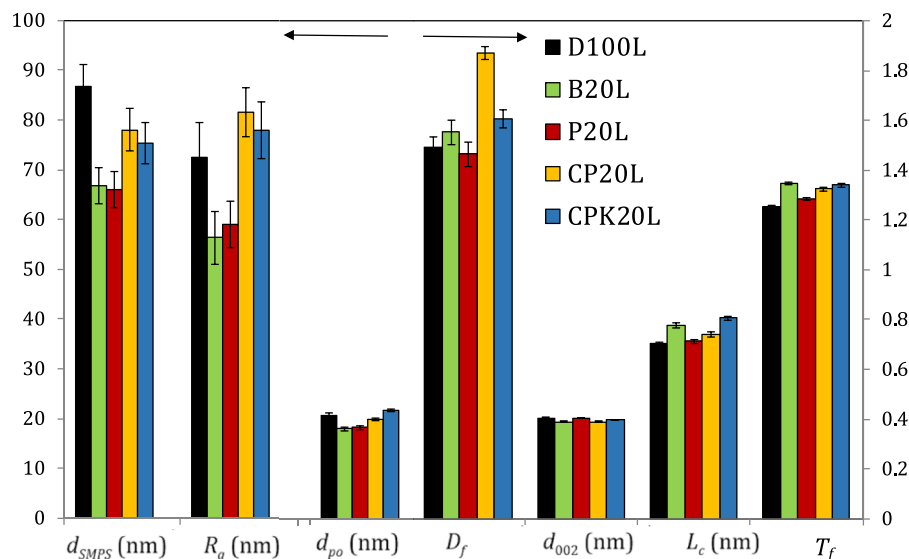
a)
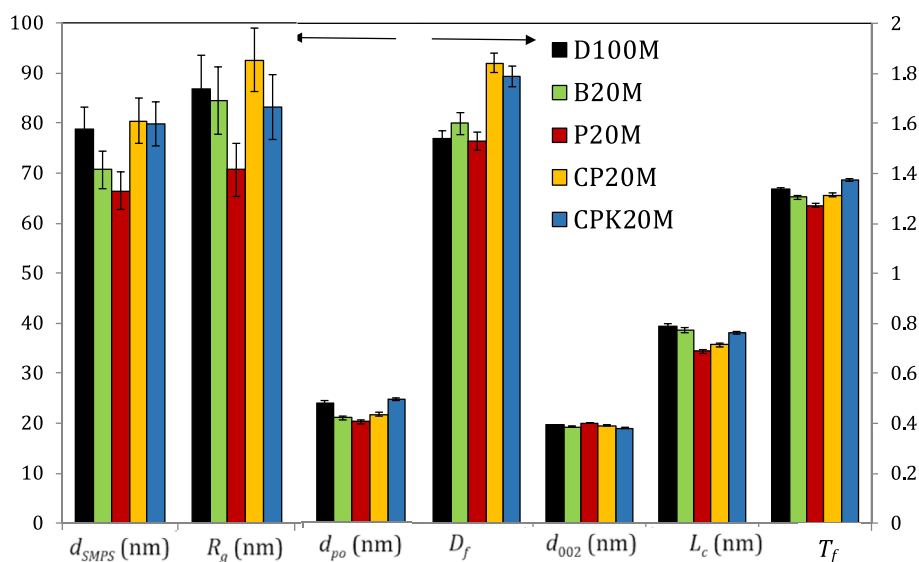
b)

Fig. 6. Particulate characteristics for different fuels at a) 2 bar and b) 4 bar IMEP.

due to the higher in-cylinder temperature, being particularly noticeable for the particles emitted from diesel fuel and ketone fuel blend combustion. Particles emitted by the oxygenated fuel blends have a smaller d_{002} that those emitted by diesel fuel for both engine loads giving an indication of a more ordered particle nanostructure coincident with results already published for other oxygenated fuels [17].

The fringe length (L_c) decreases with increasing engine load for all bio-alcohols and bio-ketone blended fuels (Fig. 6). However, the opposite effect is seen in the case of particles emitted from diesel fuel combustion. It seems that the presence of oxygenated compounds in the fuel (hydroxyl and carbonyl) prevail over the effect of increasing the formation rate of soot precursors with the engine load. In these cases, the graphene layers are shorter, probably due to oxidation in the early stages of soot and soot precursors formation that later on form the

graphene fringes. It should be noted that, in the case of cyclopentanone, the oxidation effect is more significant than in the case of alcoholic fuel blends, so it is significantly decreasing the length of the fringes with increasing engine load.

The relationship between the fringes length and the distance between their extremes is called tortuosity (T_f) [26]. This is a quantitative measure of the curvature of the fringes. T_f seems to follow the same trends than L_c with respect to the fuel used. The T_f (and L_c) of the graphene layers contained in the particles produced from oxygenated fuels is larger at low load conditions, while it is smaller at medium load conditions. The change of trends with the engine load is due to the change in temperature induced by the engine load. At medium load the in-cylinder temperature is higher than at low load and then the oxygen content from the oxygenated fuels could oxidise/break the outer

graphene layer into small fringes during the oxidation process reducing tortuosity. This was also discussed earlier justifying the smaller primary particles from the combustion of oxygenated fuel blends compared to those formed from diesel fuel combustion. The decrease in L_c, T_f and d_{po} enhance the reactivity of soot particles meaning that they will be easier to be oxidized [46,47].

4. Conclusions

The oxygen content of butanol, pentanol, cyclopentanol and cyclopentanone and the proportion of premixed combustion and higher in-cylinder temperatures are the main fuel characteristics affecting combustion and emissions. The studied oxygenated fuels decreases HC and PM emissions. Furthermore, the lower carbon to hydrogen ratio of straight-chain alcohol fuels can inhibit the formation of particles. On the other hand, the oxygen content in the molecular fuel structure and higher peak mean combustion temperature leads to an increase in NO_x emissions which could be eliminated by integrating catalytic converters. Comparing the oxygenated fuel blend components, the cyclic structure alcohol (CP20) resulted in further decrease in PM emissions compared to the straight-chain alcohols (B20 & P20). The double bond oxygen within the ketone molecular structure (CPK20) decreased the NO_x, HCs and PM emissions. Higher NO_2 concentration from all oxygenated fuels would be beneficial for lower temperature soot oxidation during the DPF regeneration. The morphology and nanostructure of the exhaust particles was influenced by the bio-alcohol and bio-ketone molecular structure and the extend of influence was different for the studied engine loads. At 2 bar IMEP, the molecular structure of fuels such as hydroxyl and carbonyl group significantly affect PM characteristics. Increased fuel/air ratio at 4 bar IMEP for all the tested fuels increases the average radius of gyration (R_g) and the average diameter of the agglomerates' primary particles (d_{po}) increasing accumulation soot production. The oxygen content in the oxygenated fuels reduced primary particle size by slowing down the particles' surface growth.

In summary, Low-carbon bio-alcohols and bio-ketones in advanced clean propulsion systems demonstrate a high potential for unveiling strategies for vehicular emissions abatement, such as their utilisation in hybrid vehicles. In the short term, this will improve air quality, overcome full electric vehicle infrastructure challenges, ensure sustainable feedstock sources, and address economic considerations.

CRediT authorship contribution statement

Omid Doustdar: Writing – review & editing, Writing – original draft, Visualization, Methodology, Investigation, Formal analysis, Data curation, Conceptualization. **Soheil Zeraati-Rezaei:** Writing – review & editing, Methodology, Investigation, Conceptualization. **Jose Martin Herreros:** Conceptualization, Investigation, Writing – review & editing, Project administration. **Francisco Javier Martos:** Methodology, Formal analysis, Investigation. **Athanasios Tsolakis:** Writing – review & editing, Supervision, Resources, Project administration, Funding acquisition, Conceptualization. **Miroslaw Lech Wyszynski:** Writing – review & editing, Supervision.

Declaration of competing interest

The authors declare that they have no known competing financial interests or personal relationships that could have appeared to influence the work reported in this paper.

Data availability

Data will be made available on request.

References

[1] Graham C, Ameya J, Felix L, Antonio G, Kelly SP. A review of current and future powertrain technologies and trends in 2020. Transportation Engineering 2021;5: 100080.

[2] (ACEA) The European Automobile Manufacturers' Association. Driving Mobility for Europe; 2023. Available from: https://www.acea.auto/fuel-pc/fuel-types-of-ne w-cars-battery-electric-12-1-hybrid-22-6-and-petrol-36-4-market-share-full-year-2 022/.

[3] David C, Giacomo T, Nicolae S, Matteo P. The challenge of forecasting the role of biofuel in EU transport decarbonisation at 2050: A meta-analysis review of published scenarios. Renew Sustain Energy Rev 2021;139:110715.

[4] European Commision. Commission Delegated Regulation (EU) on the methodology to determine the share of biofuel and biogas for transport, produced from biomass being processed with fossil fuels in a common process. Brussels; June 2023.

[5] Gautam K. Is it really the end of internal combustion engines and petroleum in transport? Appl Energy 2018;225:965–74.

[6] Abdul-Manan Amir F. N., Won Hyun-Woo, Li Yang, Sarathy S. Mani, Xie Xiaomin, Amer Amer A. Bridging the gap in a resource and climate-constrained world with advanced gasoline compression-ignition hybrids. Applied Energy 2020;267: 114936.

[7] Zeraati-Rezaei Soheil, Al-Qahtani Yasser, Herreros Jose M., Ma Xiao, Xu Hongming. Experimental investigation of particle emissions from a Dieseline fuelled compression ignition engine. Fuel 2019;251:175-86.

[8] Doustdar Omid, Zeraati-Rezaei Soheil, Herreros Jose Martin, Tsolakis Athanasios, Dearn Karl D., Wyszynski Miroslaw Lech. Tribological Performance of Biomass-Derived Bio-Alcohol and Bio-Ketone Fuels. Energies 2021;14(17):5331.

[9] Jingjing He, Hao C, Chen Yisong Su, Xin ZP, Hongming Xu, et al. Optical study on the spray and combustion of diesel cyclopentanol blend fuels on a constant volume chamber. Fuel 2022;315:123171.

[10] Paul H, Midhat T, Aaron E, Nicos L. An overview of the effects of fuel molecular structure on the combustion and emissions characteristics of compression ignition engines. Proceedings of the Institution of Mechanical Engineers, Part D: Journal of Automobile Engineering 2018;232(1):90–105.

[11] Paul H, Nicos L, Robert A, Sorin F, John R. The importance of double bond position and cis–trans isomerisation in diesel combustion and emissions. Fuel 2013;105: 477–89.

[12] Fayad MA, Tsolakis A, Fernández-Rodríguez D, Herreros JM, Martos FJ, Lapuerta M. Manipulating modern diesel engine particulate emission characteristics through butanol fuel blending and fuel injection strategies for efficient diesel oxidation catalysts. Appl Energy 2017;190:490–500.

[13] Alpaslan A. Comparative analyses of diesel–waste oil biodiesel and propanol, n-butanol or 1-pentanol blends in a diesel engine. Fuel 2016;176:209–15.

[14] Chen Hao Su, Xin HJ, Zhang Peng Xu, Hongming ZC. Investigation on combustion characteristics of cyclopentanol/diesel fuel blends in an optical engine. Renew Energy 2020.

[15] Aaron E, Nicos L, Ramanarayanan B, Alina M. Conversion of oxygenated and hydrocarbon molecules to particulate matter using stable isotopes as tracers. Combust Flame 2014;161(11):2966–74.

[16] Liming C, Leif K, Malte D, Kai L, Krithika N, Mani SS, et al. Exploring the combustion chemistry of a novel lignocellulose-derived biofuel: cyclopentanol. Part I: quantum chemistry calculation and kinetic modeling. Combust Flame 2019; 210:490–501.

[17] Fayad MA, Herreros JM, Martos FJ, Athanasios T. Role of Alternative Fuels on Particulate Matter (PM) Characteristics and Influence of the Diesel Oxidation Catalyst. Environ Sci Tech 2015;49(19):11967–73.

[18] Broday DM, Ravid R. Deposition of fractal-like soot aggregates in the human respiratory tract. J Aerosol Sci 2011;42(6):372–86.

[19] Barone Teresa L., Lall Anshuman Amit, Zhu Yifang, Yu Rong-Chung, Friedlander Sheldon K. Inertial deposition of nanoparticle chain aggregates: Theory and comparison with impactor data for ultrafine atmospheric aerosols. Journal of Nanoparticle Research 2006;8(5):669-80.

[20] Bogarra M, Herreros JM, Tsolakis A, York APE, Millington PJ, Martos FJ. Influence of on-board produced hydrogen and three way catalyst on soot nanostructure in Gasoline Direct Injection engines. Carbon 2017;120:326–36.

[21] Vander Wal Randy L, Bryg VM, Hays MD. Fingerprinting soot (towards source identification): Physical structure and chemical composition. J Aerosol Sci 2010;41 (1):108–17.

[22] Reza HM, Omid D, Athanasios T, Jonathan H. Energy-efficient heating strategies of diesel oxidation catalyst for low emissions vehicles. Energy 2021;230:120819.

[23] Magín L, Rosario B, Martos FJ. A method to determine the fractal dimension of diesel soot agglomerates. J Colloid Interface Sci 2006;303(1):149–58.

[24] Magín L, Martos FJ, Gema M-G. Geometrical determination of the lacunarity of agglomerates with integer fractal dimension. J Colloid Interface Sci 2010;346(1): 23–31.

[25] Martos FJ, Magín L, José EJ, Enrique S-R. Overestimation of the fractal dimension from projections of soot agglomerates. Powder Technol 2017;311:528–36.

[26] Kuen Y, Vander Wal Randy L, Boehman AL. Development of an HRTEM image analysis method to quantify carbon nanostructure. Combust Flame 2011;158(9): 1837–51.

[27] Rajesh KB, Muthukkumar T, Krishnamoorthy V, Saravanan S. A comparative evaluation and optimization of performance and emission characteristics of a DI diesel engine fueled with n-propanol/diesel, n-butanol/diesel and n-pentanol/ diesel blends using response surface methodology. RSC Adv 2016;6(66):61869–90.

[28] Rajesh KB, Saravanan S. Effects of iso-butanol/diesel and n-pentanol/diesel blends on performance and emissions of a DI diesel engine under premixed LTC (low temperature combustion) mode. Fuel 2016;170:49–59.

[29] Byungchul C, Xiaolong J. Individual hydrocarbons and particulate matter emission from a turbocharged CRDI diesel engine fueled with n-butanol/diesel blends. Fuel 2015;154:188–95.

[30] Cheung CS, Lei Zu, Zhen H. Regulated and unregulated emissions from a diesel engine fueled with biodiesel and biodiesel blended with methanol. Atmos Environ 2009;43(32):4865–72.

[31] Elina K, Nicos L, Martin G. The influence of various oxygenated functional groups in carbonyl and ether compounds on compression ignition and exhaust gas emissions. Fuel 2015;159:697–711.

[32] Alessandro S, Nicos L, John W, Robert A, John R. The influence of molecular structure of fatty acid monoalkyl esters on diesel combustion. Combust Flame 2009;156(7):1396–412.

[33] Herreros JM, Schroer K, Sukjit E, Tsolakis A. Extending the environmental benefits of ethanol–diesel blends through DGE incorporation. Appl Energy 2015;146: 335–43.

[34] Gowtham M, Mohan CG, Prakash R. Effect of n-butanol fumigation on the regulated and unregulated emission characteristics of a diesel engine. Fuel 2019; 242:84–95.

[35] Ruijun Zu, Cheung CS, Zuohua H, Xibin W. Regulated and unregulated emissions from a diesel engine fueled with diesel fuel blended with diethyl adipate. Atmos Environ 2011;45(13):2174–81.

[36] Francisco P, Bermúdez VR, Bernardo T, Linares WG. Hydrocarbon emissions speciation in diesel and biodiesel exhausts. Atmos Environ 2009;43(6):1273–9.

[37] Gowtham M, Prakash R. Control of regulated and unregulated emissions from a CI engine using reformulated nano fuel emulsions. Fuel 2020;271:117596.

[38] Wei L, Cheung CS, Ning Z. Effects of biodiesel-ethanol and biodiesel-butanol blends on the combustion, performance and emissions of a diesel engine. Energy 2018; 155:957–70.

[39] Saravanan S, Nagarajan G, Anand S, Sampath S. Correlation for thermal NOx formation in compression ignition (CI) engine fuelled with diesel and biodiesel. Energy 2012;42(1):401–10.

[40] Cheung CS, Yage Di, Zuohua H. Experimental investigation of regulated and unregulated emissions from a diesel engine fueled with ultralow-sulfur diesel fuel blended with ethanol and dodecanol. Atmos Environ 2008;42(39):8843–51.

[41] Elina K, Nicos L, Martin G. Compression ignition and pollutant emissions of large alkylbenzenes. Fuel 2016;172:200–8.

[42] Sukjit E, Herreros JM, Piaszyk J, Dearn KD, Tsolakis A. Finding Synergies in Fuels Properties for the Design of Renewable Fuels – Hydroxylated Biodiesel Effects on Butanol-Diesel Blends. Environ Sci Tech 2013;47(7):3535–42.

[43] Magín L, Octavio A, Herreros JM. Emissions from a diesel–bioethanol blend in an automotive diesel engine. Fuel 2008;87(1):25–31.

[44] Lapuerta Magín.; Ballesteros, Rosario.; Martos, Francisco J.; . The effect of diesel engine conditions on the size and morphology of soot particles. International Journal of Vehicle Design (IJVD) 2009;50(1/2/3/4):91-106.

[45] Xiaochen W, Ying W, Yuanqi B, Peng W, Dongxing W, Funan G. Effects of 2,5-dimethylfuran addition on morphology, nanostructure and oxidation reactivity of diesel exhaust particles. Fuel 2019;253:731–40.

[46] Magín L, Fermín O, Agudelo JR, Boehman AL. Effect of fuel on the soot nanostructure and consequences on loading and regeneration of diesel particulate filters. Combust Flame 2012;159(2):844–53.

[47] Vander Wal Randy L, Tomasek AJ. Soot oxidation: dependence upon initial nanostructure. Combust Flame 2003;134(1):1–9.